JOURNAL OF Materials CHEMISTRY

Crystal structure of the thallium strontium cobaltite $TlSr_2CoO_5$ and its relationship to the electronic properties†

Jean-Pierre Doumerc,*[a] Martine Coutanceau,[a] Alain Demourgues,[a] Erik Elkaim,[b] Jean-Claude Grenier[a] and Michel Pouchard[a]

[a]*ICMCB-CNRS, 87 avenue du Dr. A. Schweitzer, 33608 Pessac, France. E-mail: doumerc@icmcb.u-bordeaux.fr*
[b]*LURE, Bât 209D, Centre Universitaire Paris-Sud, B.P. 34, 91898 Orsay Cedex, France*

Received 5th May 2000, Accepted 26th June 2000
First published as an Advance Article on the web 5th October 2000

The complex cobaltite $TlSr_2CoO_5$ undergoes a first-order metal–insulator phase transition at room temperature. The structures of the high temperature (HT) and low temperature (LT) phases have been refined on powder samples using electron diffraction, X-ray diffraction and EXAFS. The HT-phase is isostructural with the so-called 1201-type cuprate. The unit cell is tetragonal (space group *P*4/*mmm*) and cobalt occupies a highly elongated octahedron. At low temperature, a commensurate modulation of the oxygen positions sets in such that two sites are available for cobalt, in the ratio 1 to 2. The sizes and the distortions of these two sites differ in such a way that a different electronic configuration of cobalt is stabilized in each. This effect is described as a spin state disproportionation (SSD). Long range ordering of these two spin states (SSO) is compared to the charge ordering (CO) effect and SSO seems to play a role as important for cobaltites(III) as CO does for nickelates or manganites.

1 Introduction

The thallium strontium cobaltite $TlSr_2CoO_5$ undergoes a first-order metal–insulator transition near room temperature characterized by an hysteresis loop and steep changes in the temperature dependences of the magnetic susceptibility and of the electrical resistivity.[1] The electrical resistivity, which is larger than $10^6\ \Omega$ cm at 100 K, decreases as the temperature (T) increases, reaching a value of 2 Ω cm at 270 K, and then rapidly drops to 0.05 Ω cm near room temperature, becoming nearly temperature independent. The Seebeck coefficient is positive at low temperature, increases with T, exhibits a maximum of 200 $\mu V\ K^{-1}$ at 150 K, then decreases and changes its sign at room temperature, reaching a value of $-15\ \mu V\ K^{-1}$ at 310 K that very slightly and linearly decreases with temperature. The molar magnetic susceptibility ($\chi_M = 8 \times 10^{-3}\ mol^{-1}$ at 4 K) exhibits a peak at 150 K, attributed to the onset of antiferromagnetic ordering, but does not vary much between liquid helium and room temperature, where it sharply increases, almost doubling its value. Above 300 K, χ_M rapidly decreases following a Curie–Weiss law with a Curie constant of 1.7 emuCGS K mol^{-1} and a large positive Weiss constant of 200 K, denoting dominant very strong ferromagnetic interactions that can be ascribed to a double exchange mechanism. In conclusion, the low temperature (LT) phase is an *antiferromagnetic p-type insulator* whereas the high temperature (HT) phase is an *n-type metal* with dominant *ferromagnetic* interactions.

In a preliminary investigation the HT- and LT-phases were both described as isostructural with the tetragonal form of the so-called 1201 member of the well-known series of thallium strontium calcium cuprates.[2] The tetragonal unit cell undergoes a significant decrease in volume at the transition, the HT form being denser than the LT form.

Extended X-ray absorption fine structure (EXAFS) studies reveal a much wider dispersion of the Co–O distances at low temperature than at high temperature. Electron diffraction (ED) patterns recorded below *ca.* 250 K clearly show weak spots indicating a modulation of the structure. Both series of results are reported below.

Since the difference between the structures of the HT- and LT-phases appears minimal, there is no hope of growing single crystals in the very near future and amounts of the compound large enough to allow neutron diffraction experiments to be performed are not yet available, high resolution XRD data were recorded using synchrotron radiation in order to carry out a refinement of the structure by the Rietveld method on the basis of the unit cell and space group deduced from the ED results.

The purpose of this paper is to account for the whole set of results and to discuss the relationship between the structural and physical properties.

2 Experimental

Sample preparation and chemical analysis have been described previously.[2] Starting materials were Tl_2O_3, SrO and $Sr_2Co_2O_5$ in the ratio 1 : 2 : 1. The homogenized mixture was heated in a sealed gold tube at 900 °C for 3 h. Such conditions are not far from those used for preparing thallium cuprates. Generally, loss of thallium is observed, requiring a determination of the composition and of the oxidation state of cobalt. The Tl, Sr and Co contents were determined at the Service Central d'Analyses du CNRS.[3] Two successive iodometric titrations were used for the determination of the oxidation states of Tl and Co.[2] Writing the general formula of the material as:

$$Tl_{1-\delta}Sr_2Co^{3+}_{1-\tau}Co^{4+}_{\tau}O_{5-\varepsilon}$$

the most probable values of δ, τ and ε for the investigated sample are 0.07, 0.05 and 0.07, respectively.

A TEM study was carried out with a Jeol 2000 FX microscope equipped with a double tilt sample holder. The temperature of the sample was controllable between 100–350 K.

†Basis of a presentation given at Materials Discussion No. 3, 26–29 September, 2000, University of Cambridge, UK.

 DOI: 10.1039/b003198o

High resolution diffraction (HRD) data were collected at LURE (Laboratoire pour l'Utilisation du Rayonnement Electromagnétique in Orsay) on the DCI storage ring at the beam line DW22.[4]

Absorption spectra for the EXAFS study were recorded at 10, 100, 250 and 330 K between 7650 and 8750 eV with a step of 0.3 eV and a counting time of 2 s.

3 Results

3.1 The high temperature tetragonal t-phase

At room temperature, the product contains two phases, but above *ca.* 310 K, only a single phase remains in the XRD patterns. It is isostructural with the tetragonal form of the analogous cuprate[5] (space group: *P*4/*mmm*). For the purposes of comparison with the LT-phase, selected ED patterns

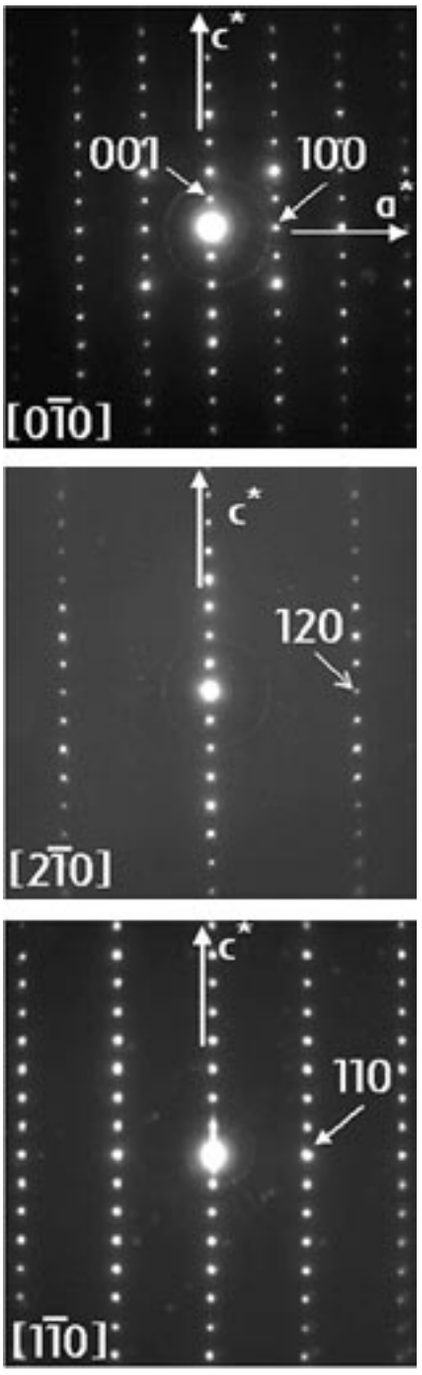

Fig. 1 ED patterns of a crystal of the HT tetragonal form of $TlSr_2CoO_5$ recorded at 350 K.

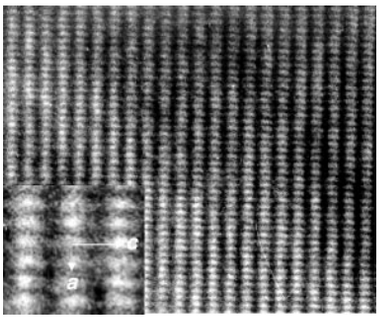

Fig. 2 High resolution image of the HT tetragonal form of $TlSr_2CoO_5$ along the [0$\bar{1}$0] zone axis, showing the absence of extended defects.

recorded at 350 K are given in Fig. 1. These were obtained by tilting around the c^* axis, which can be easily identified, and indexed with a tetragonal primitive cell. No additional reflections were observed and the measured cell parameters are close to the expected values ($a=0.375$, $c=0.877$ nm).[2] Reflection conditions agree with the tetragonal *P*4/*mmm* space group. A typical high resolution image shows the absence of any extended defects (Fig. 2).

As both the HT- and LT-phases coexist at room temperature, XRD data were collected at 373 K on a Siemens diffractometer using a copper anticathode and equipped with a platinum heating sample holder, for 2θ varying from 15 to 99° in steps of 0.015°. Structural parameters were refined using the Rietveld method and the Fullprof program.[6] Difficulties arose from the complex upward-bending shape of the background at small diffraction angles ($2\theta<40°$) and from the presence of the strong 200 peak of platinum at 46.5°, which was introduced as a second phase; the background was modeled by linear interpolation between 25 given points. Experimental and calculated diffractograms are given in Fig. 3 and atomic positions are reported in Table 1. The fractional occupancy of the thallium site was also refined and the Tl deficiency determined (Table 1) was consistent with the results of chemical analysis. Relevant interatomic distances are given in Table 2, a drawing of the structure is presented in Fig. 4 and the coordination environment of the Co ions is shown in Fig. 5. Table 2 and Fig. 5 highlight the fact that the oxygen octahedron surrounding the Co atoms is highly elongated. A similar distortion has been reported for $Pb_{0.63}Cu_{0.37}Sr_2CoO_5$.[7] This elongation should be correlated to very short apical Tl–O bond lengths, which is a general feature of thallium–oxygen bonding. Such short Tl–O distances have previously been reported for thallium cuprates[8] and ferrites.[9,10] It should also be noted that Tl atoms lie on an inversion centre (1a site),

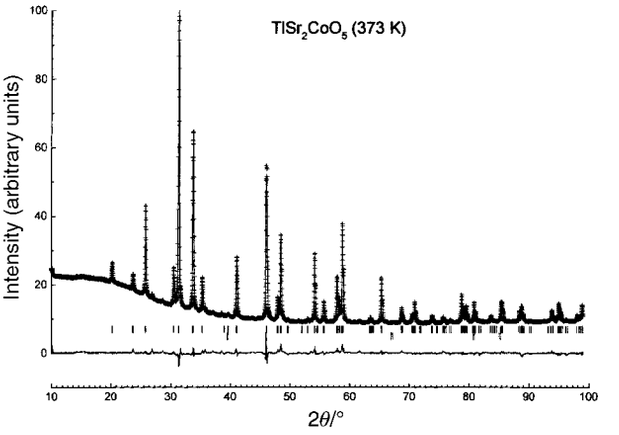

Fig. 3 Measured (discrete points) and calculated (solid line) XRD intensities and their differences for $TlSr_2CoO_5$ at 373 K. The strong peak at 46.5° is the 200 peak of the platinum sample holder.

Table 1 Atomic positions in the high temperature form of $TlSr_2CoO_5$ and refinement parameters[a]

Atom	Site multiplicity Wyckoff letter	x	y	z	Fractional occupancy
Tl	1a	0	0	0	0.93(5)
Sr	2h	0.5	0.5	0.2903(3)	1
Co	1b	0	0	0.5	1
O1	2g	0	0	0.232(3)	1
O2	1c	0.5	0.5	0	1
O3	2e	0	0.5	0.5	1

[a]Cell parameters/nm: $a=0.37571(1)$; $c=0.87920(2)$. Space group: $P4/mmm$. Isotropic overall temperature factor/Å^2: $B=0.15$. Profile parameters: $U=0.072(3)$; $V=-0.076(3)$; $W=0.035(1)$; η(pseudo-Voight)$=0.764(7)$. Conventional Rietveld R-factors (%): $R_p=13.3$; $R_{wp}=9.5$; $\chi^2=14$; $R_{Bragg}=8.1$; $R_f=8.8$.

Table 2 Main interatomic distances in the high temperature form of $TlSr_2CoO_5$

Tl–O1	0.2045(8) (×2)
Tl–O2	0.2651(1) (×4)
Co–O1	0.2346(8) (×2)
Co–O3	0.1875(1) (×4)
Co–Sr	0.3230(1) (×8)
Sr–O1	0.2705(2) (×4)
Sr–O2	0.2550(1) (×1)
Sr–O3	0.2634(1) (×4)

unlike in cuprates where they are slightly shifted within the ***ab*** plane from this ideal position.

3.2 The low temperature orthorhombic o-phase

3.2.1 Electron diffraction. ED patterns were recorded at 100 K and are reported in Fig. 6 for two zone axes. Patterns A to C can be compared with the corresponding ones in Fig. 1. All the patterns have the following main features: (i) intense spots corresponding to a tetragonal lattice similar to that used for describing the HT-phase and (ii) weaker additional spots of variable intensities which cannot be indexed using the space group $P4/mmm$. However, they are always commensurate with the basic tetragonal network and are located in such a way that d_{120} and d_{110} are tripled (patterns B, C and D). Comparing the patterns of various crystals, changing the beam section and shifting the samples reveals that the crystals are actually twinned, the average size of microdomains being smaller than 0.5 μm. The twins correspond to a rotation of π/2 radians around the c axis, which is not surprising as the sublattice is tetragonal. It was not possible to directly observe a crystal with a zone axis parallel to $\boldsymbol{c}_t$ (the index t refers to the tetragonal sublattice), but the whole reciprocal lattice can be built from the patterns obtained with other orientations. The ($\boldsymbol{a}_t^*$, $\boldsymbol{b}_t^*$) plane deduced in this way is shown in Fig. 7. All the diffraction patterns can be indexed assuming that two perpendicular basic reciprocal lattices are superposed, as shown in Fig. 7.

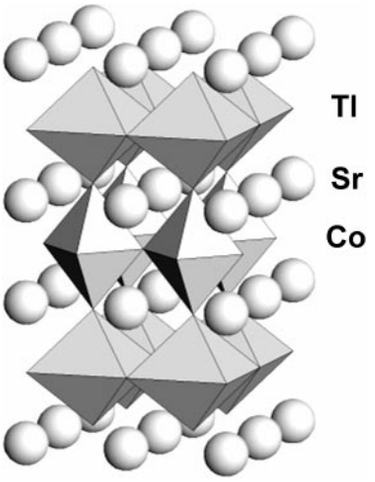

Fig. 4 Structure of the high temperature form of $TlSr_2CoO_5$.

The whole set of patterns can be interpreted using a modulation vector:

$$\boldsymbol{q}^* = 1/3\boldsymbol{a}_t^* + 1/3\boldsymbol{b}_t^* + 1/2\boldsymbol{c}_t^*$$

In other words, each intense spot of the tetragonal sublattice is accompanied, in the direction of the $\boldsymbol{q}^*$ vector, by three spots of decreasing intensities, the third having a vanishing intensity. This $\boldsymbol{q}^*$ vector is drawn in the pattern of Fig. 8. Using $\boldsymbol{q}^*$ makes it possible to index all the spots with four indices, h, k, l and m, where m stands for the satellite order. For instance, some spots in Fig. 8 are indexed in this way.

3.2.2 XRD: structure refinement. As the modulation is commensurate, refinement of the structure can be approximated using a superstructure and a 3D space group. Two possible supercells are drawn in Fig. 7. The larger one (the smaller in real space) is monoclinic (dotted line in Fig. 7). Diffraction conditions for $0k0$ are $k=2n$, leading to two possible space groups: $P2_1$ and $P2_1/m$. However, refinements carried out using these models were not satisfactory: for instance, the R_{Bragg} factor always remained larger than 12%.

To overcome this difficulty we chose a larger (in real space), but more symmetric supercell, also shown in Fig. 7 (solid line). This cell is orthorhombic and related to the tetragonal subcell by:

$$\begin{pmatrix} a_o* \\ b_o* \\ c_o* \end{pmatrix} = Q_o \begin{pmatrix} a_t* \\ b_t* \\ c_t* \end{pmatrix} \quad \text{with } Q_o = \begin{pmatrix} 1/2 & -1/2 & 0 \\ 1/6 & 1/6 & 0 \\ 0 & 0 & 1/2 \end{pmatrix}$$

Reflection conditions for hkl are $h+k=2n$, denoting a base-centered Bravais lattice of C type, and for $h0l$, $l=2n$. Two space groups are possible: $Cmcm$ and $Cmc2_1$. As usual, we chose the more symmetric of the two, *i.e.* $Cmcm$. The starting atomic coordinates were calculated from those found for the HT-phase using the relationship:

$$\begin{pmatrix} x_o \\ y_o \\ z_o \end{pmatrix} = Q_o \begin{pmatrix} x_t \\ y_t \\ z_t \end{pmatrix}$$

For the refinement, we assumed the same thermal factors for atoms of the same nature. The synchrotron radiation wavelength was equal to 0.106942 nm. The data were recorded for $5 \leqslant 2\theta \leqslant 75°$, with a step size of 0.02°. The results of the refinement are given in Table 3 and selected interatomic distances in Table 4.

Measured and calculated XRD patterns are displayed in Fig. 9.

3.2.3 Description of the LT-phase structure. A perspective view of the LT-phase structure is reproduced in Fig. 10. If only

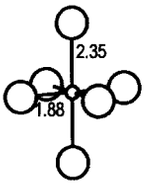

Fig. 5 Environment of the cobalt atoms in the high temperature form of $TlSr_2CoO_5$.

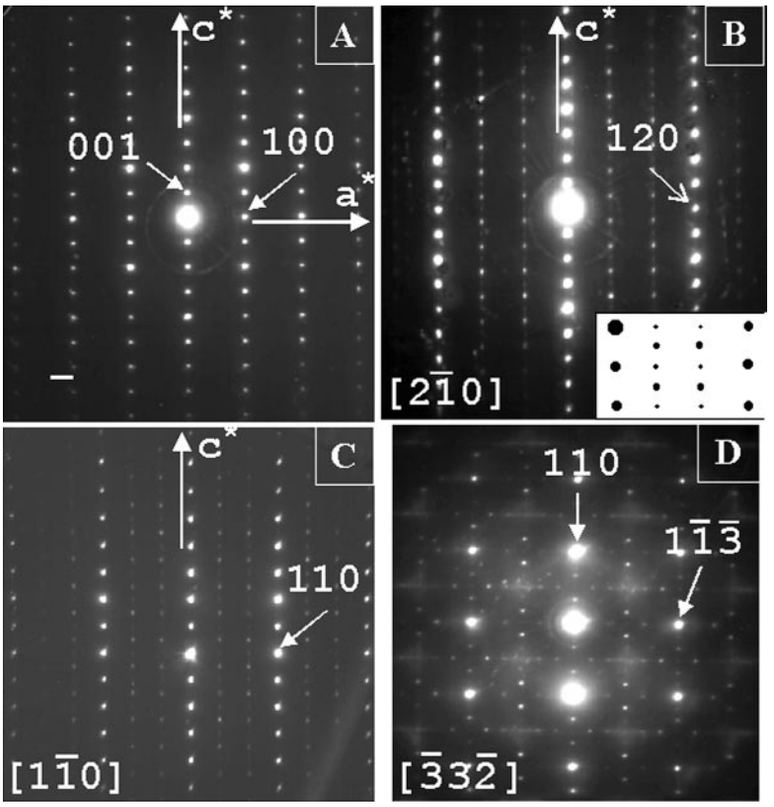

Fig. 6 ED patterns of the LT-phase of $TlSr_2CoO_5$ recorded at 100 K.

Tl–O distances shorter than 0.27 nm are taken into account, the Tl1 and Tl2 thallium atoms are located in a distorted pyramid. The third Tl atom, Tl3, occupies a very distorted octahedral site with two short apical Tl–O distances. The Tl–O distances are in agreement with those reported earlier for thallium cuprates[8] and reflect the ability of thallium to accommodate various more or less distorted sites, as, for instance, in $Ba_2Tl_2O_5$ (distorted tetrahedron),[11] $Sr_4Tl_2O_7$ (square), $Ca_2Tl_2O_5$[12] and $Sr_2Tl_2O_5$[13] (distorted octahedron). It should be pointed out that two apical Tl–O distances are very short, allowing a significant elongation of the CoO_6 octahedra along the c axis. Refining the fractional site occupancy for Tl provides a value smaller than unity (0.97), in agreement with the chemical analysis discussed above, but larger than the value found for the tetragonal HT-phase (0.93). We will assume a final value of 0.95 ± 0.02. Further investigation will be required in order to gain better control of the Tl stoichiometry and sample homogeneity, but it appears difficult to avoid Tl loss during synthesis.

Two sites, labeled I and II, were found for the cobalt atoms. Site I is a highly elongated octahedron with four very short Co–O distances of 0.179 nm in the ($\boldsymbol{a}_o$, $\boldsymbol{b}_o$) plane. Site II is larger and more distorted with one long Co–O distance of 0.247 nm, giving rise to a coordination of 5+1 (Fig. 11).

Fig. 12 shows the perovskite-type CoO_3 layers at $z=0$ where polyhedra corresponding to site I and II are distinguished. This drawing shows the way in which the two kinds of cobalt atoms are ordered within the layers. The larger II sites form zigzag chains along the $\boldsymbol{a}_o$ direction separated by the smaller I sites.

Fig. 12 also displays the succession of cobalt and oxygen atoms along the $\boldsymbol{a}_t = (1/2)\boldsymbol{a}_o + (1/6)\boldsymbol{b}_o$ direction. It will be noted that the Co atoms remain regularly spaced as in the HT tetragonal form, whereas the oxygen atoms are shifted from the central position with a periodicity commensurate with the cobalt distribution, but three times smaller.

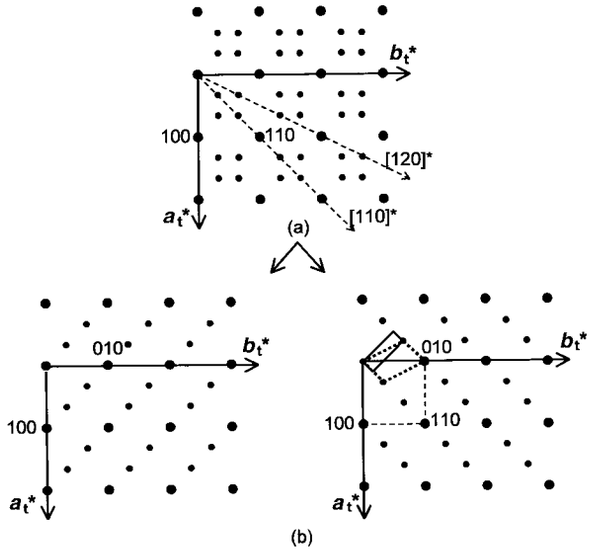

Fig. 7 ($\boldsymbol{a}_t$*, $\boldsymbol{b}_t$*) plane deduced from various experimental patterns (a) and its decomposition into two orthogonal reciprocal planes (b).

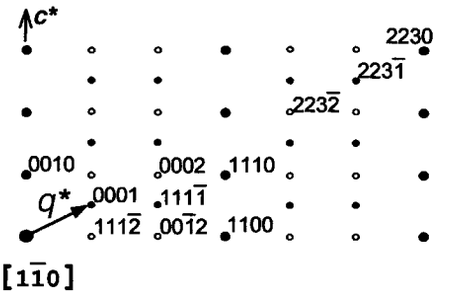

Fig. 8 Drawing of an ED pattern along the [1$\bar{1}$0] zone axis where open circles represent spots of weaker intensity and showing the $\boldsymbol{q}$* modulation vector. Spot indexing refers to the tetragonal subcell. The 4th index is the satellite order.

Table 3 Atomic positions in the low temperature form of $TlSr_2CoO_5$, profile parameters and reliability factors[a]

Atom	Site multiplicity Wyckoff letter	x	y	z	B/Å^2	Fractional occupancy
Tl1	4c	0	0.0183(3)	0.25	0.86(4)	0.973(4)
Tl2	4c	0	0.3154(3)	0.25	0.86(4)	0.973(4)
Tl3	4c	0	0.6660(3)	0.25	0.86(4)	0.973(4)
Co1	4a	0	0	0	0.189(4)	1
Co2	8f	0	0.3343(6)	−0.0065(4)	0.189(4)	1
Sr1	8f	0	0.5013(6)	0.3949(4)	0.14(5)	1
Sr2	8f	0	0.1684(6)	0.3980(3)	0.14(5)	1
Sr3	8f	0	−0.1662(6)	0.3938(3)	0.14(5)	1
O1	8f	0	0.0052(26)	0.3749(23)	0.46(23)	1
O2	8f	0	0.3461(26)	0.3667(18)	0.46(23)	1
O3	8f	0	−0.3224(29)	0.3796(19)	0.46(23)	1
O4	4c	0	0.5307(30)	0.25	0.46(23)	1
O5	4c	0	0.1638(35)	0.25	0.46(23)	1
O6	4c	0	−0.1868(29)	0.25	0.46(23)	1
O7	8d	0.25	0.25	0	0.46(23)	1
O8	16h	0.2231(60)	0.0840(15)	−0.0051(12)	0.46(23)	1

[a]Cell parameters/nm: $a=0.53311(2)$; $b=1.59697(4)$; $c=1.75422(4)$. Space group: *Cmcm*. Profile parameters: $U=0.065(5)$; $V=-0.021(3)$; $W=0.0107(4)$; η(pseudo-Voight)$=0.108(7)$. Conventional Rietveld *R*-factors (%): $R_p=14.7$; $R_{wp}=18.1$; $\chi^2=8.3$; $R_{Bragg}=8.4$; $R_f=11.2$.

3.2.4 EXAFS study. The EXAFS study has been carried out at the cobalt K-edge ($E_K=7710$ eV). For Fourier analysis the photoelectron wave vector ***k***-window spanned from 60 to 135 nm^{-1} and the real ***R***-space window from 0.15 to 0.45 nm.

Fourier transforms (FT) show four peaks, with a shoulder on one of them, which can be directly ascribed to the first five coordination shells of cobalt atoms associated with Co–O_{xy} (the subscript *xy* refers to equatorial oxygen atoms), Co–O_z

Table 4 Selected interatomic distances in the low temperature form of $TlSr_2CoO_5$

Bond	Distance/nm
Tl1–O1	0.2201(40) (×2)
Tl1–O4	0.2673(4) (×2)
Tl1–O5	0.2324(55) (×1)
Tl1–O6	0.3277(47) (×1)
Tl2–O2	0.2105(32) (×2)
Tl2–O4	0.3438(50) (×1)
Tl2–O5	0.2422(55) (×1)
Tl2–O6	0.2660(1) (×2)
Tl3–O3	0.2280(33) (×2)
Tl3–O4	0.2160(48) (×1)
Tl3–O5	0.2666(1) (×2)
Tl3–O6	0.2350(47) (×1)
Co1–O1	0.2196(41) (×2)
Co1–O8	0.1795(28) (×4)
Co2–O2	0.2470(32) (×1)
Co2–O3	0.2006(34) (×1)
Co2–O7	0.1898(7) (×2)
Co2–O8	0.1981(30) (×2)
Sr1–O1	0.2689(5) (×2)
Sr1–O2	0.2528(42) (×1)
Sr1–O3	0.2827(47) (×1)
Sr1–O4	0.2585(12) (×1)
Sr1–O8	0.2668(26) (×2)
Sr1–O8	0.2766(26) (×2)
Sr2–O1	0.2637(43) (×1)
Sr2–O2	0.2891(42) (×1)
Sr2–O3	0.2689(5) (×2)
Sr2–O5	0.2597(6) (×1)
Sr2–O7	0.2584(7) (×2)
Sr2–O8	0.2601(25) (×2)
Sr3–O1	0.2757(43) (×1)
Sr3–O2	0.2715(6) (×2)
Sr3–O3	0.2509(47) (×1)
Sr3–O6	0.2545(9) (×1)
Sr3–O7	0.2653(6) (×2)
Sr3–O8	0.2507(25) (×2)

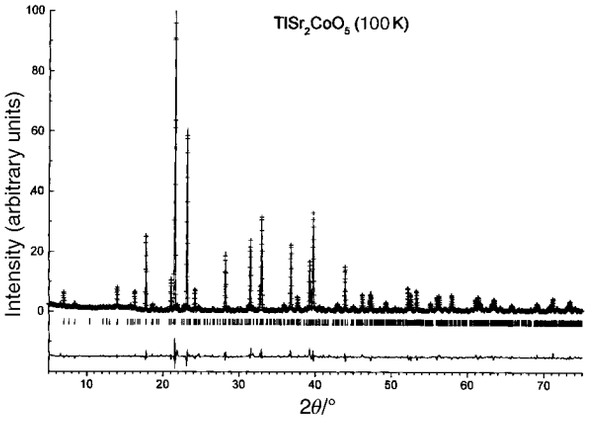

Fig. 9 Measured (discrete points) and calculated (solid line) XRD intensities for $TlSr_2CoO_5$ at 100 K. Differences between measured and calculated values are also displayed.

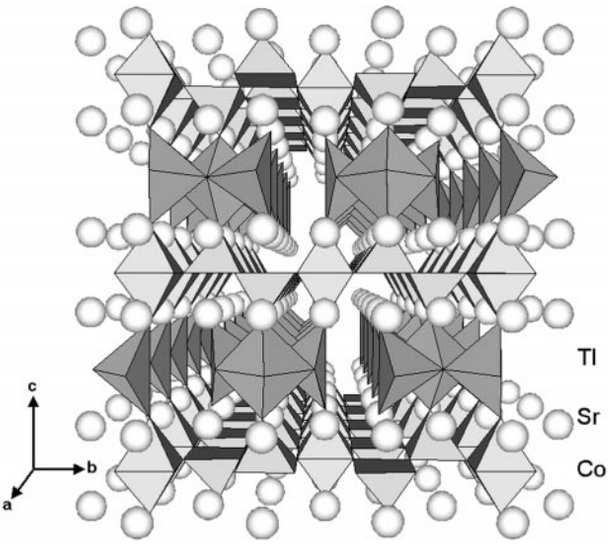

Fig. 10 Perspective drawing of the LT-phase structure. Differences compared to the HT-phase are stressed by taking into account Co–O distances shorter than 0.24 nm and Tl–O distances shorter than 0.3 nm for the determination of coordination polyhedra around Co and Tl, respectively.

Table 5 Results of the EXAFS data analysis at 330 K assuming single scattering

Distances/nm		$2\sigma^2/10^{-2}$ nm^2
Co–O_{xy}	0.184 ± 0.001	0.004
Co–O_z	0.224 ± 0.001	0.008
Co–Sr	0.316 ± 0.002	0.020
Co–Co1	0.378 ± 0.002	0.000
Co–Tl	0.438 ± 0.002	0.013

Table 6 Cartesian coordinates of atoms surrounding the central cobalt atom used for multiple scattering calculations

	x	*y*	*z*	*d*
Co	0	0	0	
$O_{xy}1$	*a*/2	0	0	*a*/2
$O_{xy}2$	0	*a*/2	0	*a*/2
O_z	0	0	*z*	*z*
Sr1	*a*/2	*a*/2	*a*/2	$\sqrt{3}a/2$
Sr2	*a*/2	*a*/2	−*a*/2	$\sqrt{3}a/2$
Sr3	*a*/2	−*a*/2	*a*/2	$\sqrt{3}a/2$
Sr4	−*a*/2	*a*/2	*a*/2	$\sqrt{3}a/2$
Co1	*a*	0	0	*a*
Co2	0	−*a*	0	*a*
Tl	0	0	*c*/2	*c*/2

(the subscript *z* refers to apical oxygen atoms), Co–Sr, Co–Co and Co–Tl distances, respectively.

3.2.4.1 EXAFS study at 330 K. Using the lattice parameters of the tetragonal unit cell of the HT-phase, the EXAFS spectra were first refined assuming a single scattering process. Eleven parameters have been refined (five radial distances, their respective Debye–Waller factors and the edge energy). Final values are given in Table 5 and EXAFS oscillations with corresponding FT are displayed in Fig. 13a. The calculated peak corresponding to the third coordination shell associated with the Co–Co distances is much smaller than the experimental one. This discrepancy should be related with the result of the refinement leading to a value of the Co–Co distance that is not twice the Co–O one (Table 6) as one might have expected from the above structural model and with a vanishing value of the Debye–Waller factor. In order to improve the fitting we have taken into account second- and third-order multiple scattering: the existence of linear –Co–O–Co–O– chains within the CoO_2 layers could favor such effects. For that purpose we have considered the atomic environment of cobalt given in Table 6 where the parameters *a*, *c* and *z* are to be refined. Origin shift and the ten coordination shells have been refined in a first step then, in a second run, their associated Debye–Waller factors. Results are given in Table 7 and EXAFS oscillations with corresponding FT are displayed in Fig. 13b. Second- and third-order scattering are mainly significant for the Co–Co coordination shell.[14]

3.2.4.2 Temperature dependence of EXAFS. Fig. 14 shows the FT of EXAFS spectra recorded at 10, 100, 250 and

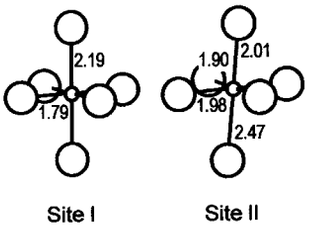

Fig. 11 Environment of the cobalt atoms in the two Co sites of the low temperature form of $TlSr_2CoO_5$.

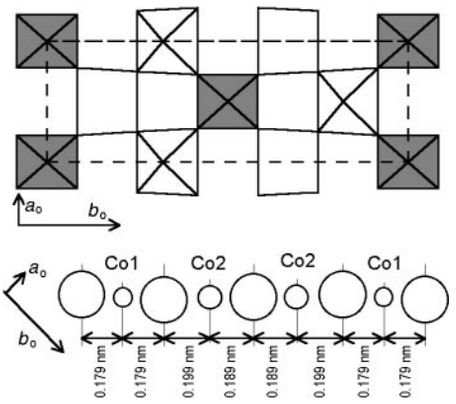

Fig. 12 CoO_2 layer at $z = 0$ showing the ordering of site I (darker) and site II and the modulation of the Co–O distances along the $\boldsymbol{a}_t$ direction.

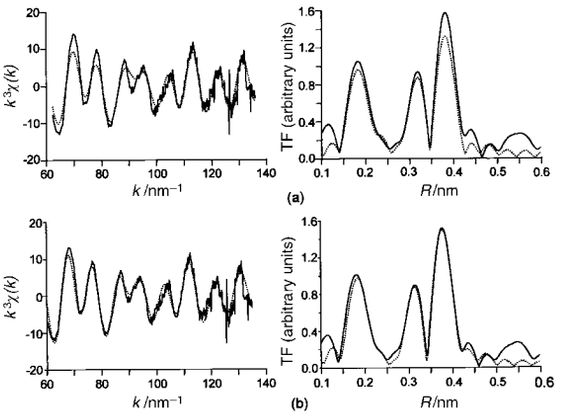

Fig. 13 Experimental (solid line) and calculated (dotted line) EXAFS spectra and their respective Fourier transforms for $TlSr_2CoO_5$, assuming single (a) or multiple diffusion (b).

330 K. The behavior of the peaks related to the Co–Co, Co–Sr and Co–Tl coordination shells seems normal, since the Debye–Waller factor decreases with decreasing temperature, which leads to the increase of the peak intensity that can be seen in Fig. 14. Conversely, the intensity of the Co–O_{xy} peak drops significantly as the temperature is reduced from 330 to 250 K, although there is little additional change upon further cooling. Obviously, such behavior reflects the sharp first-order phase transition occurring at room temperature and is in excellent agreement with the XRD results. This confirms that the structural change is mainly due to a modulation of the Co–O distances, as only the corresponding peaks do not follow the anticipated simple thermal effect.

4 Discussion

As already mentioned in the introduction, the difference between the XRD pattern of the HT tetragonal phase and that

Table 7 Results of the EXAFS data analysis at 330 K for $TlSr_2CoO_5$, assuming multiple scattering

Distances/nm		$2\sigma^2/10^{-2}$ nm^2
Co–O_z	0.228 ± 0.001	0.013
Co–$O_{xy}1$	0.187 ± 0.001	0.004
Co–$O_{xy}2$	0.186 ± 0.001	0.004
Co–Sr1	0.321 ± 0.002	0.015
Co–Sr2	0.319 ± 0.002	0.018
Co–Sr3	0.319 ± 0.002	0.020
Co–Sr4	0.320 ± 0.002	0.019
Co–Co1	0.374 ± 0.002	0.007
Co–Co2	0.374 ± 0.002	0.009
Co–Tl	0.438 ± 0.002	0.024

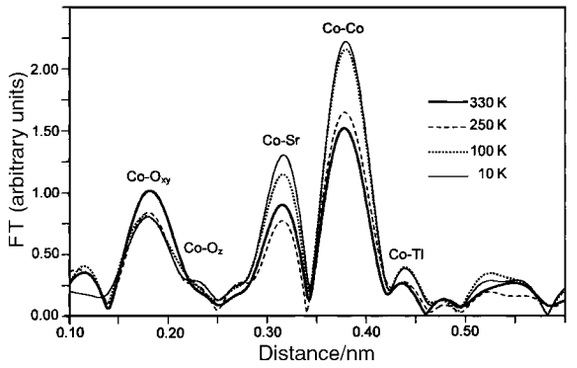

Fig. 14 Fourier transforms of EXAFS oscillations of $TlSr_2CoO_5$ at 10, 100, 250 and 330 K.

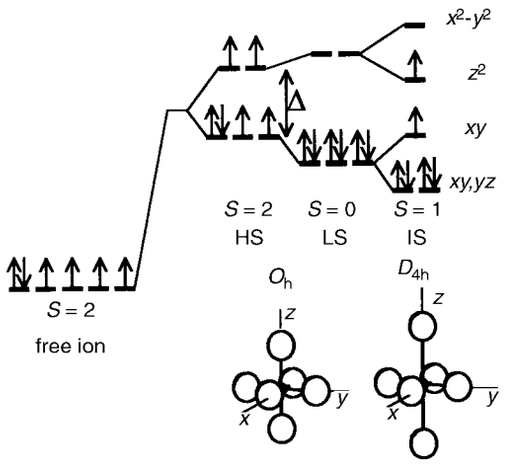

Fig. 15 Electronic configurations of Co^{3+} ions with respect to site symmetry.

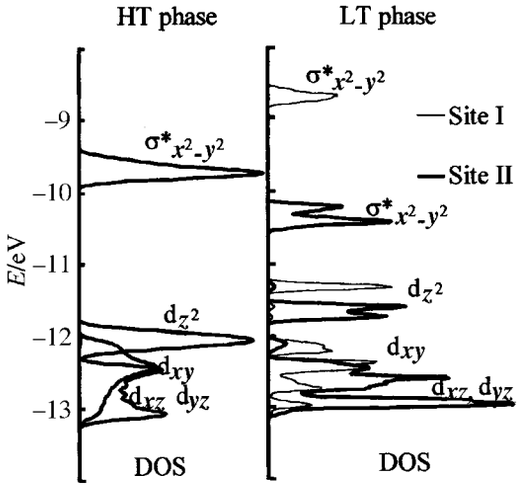

Fig. 16 d-orbital shift and splitting for cobalt in site I and site II of the LT-phase with respect to the HT-phase.

of the LT orthorhombic phase is very small. The determination of the structures as well as the EXAFS study show that it mainly results from the change in the oxygen atom positions. We have found two sites for the Co atoms markedly differing in symmetry, distortion and even the average Co–O distances (or the coordination number). The average Co–O bond length is 0.193 nm for site I and 0.204 nm for site II, if we assume sixfold coordination (0.195 nm for fivefold coordination of site II). This large difference in the Co surroundings must give rise to different electronic configurations. Obviously, disproportionation of Co^{3+} into Co^{2+} and Co^{4+} would give an equal amount

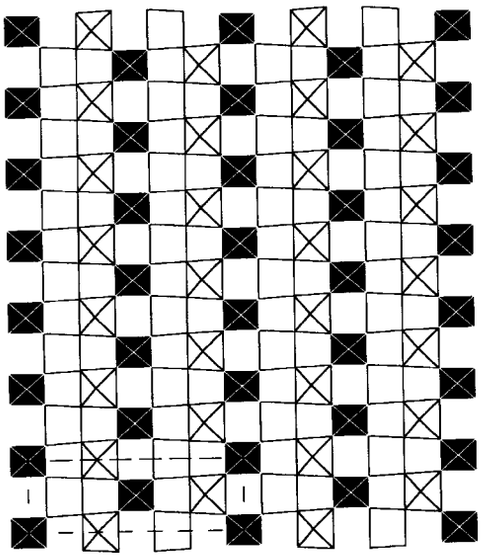

Fig. 17 Drawing of the $z=0$ CoO_2 layer over several unit cells showing the long range ordering of Co atoms.

of sites I and II against an actual ratio of 1 : 2. Therefore, such a charge disproportionation does not take place and, on the basis of ideas already proposed by Goodenough,[15] *e.g.* for $LaCoO_3$,[16] we use the concept of *spin state disproportionation* (SSD) to account for the splitting of a single average spin state at high temperature into two different spin states at low temperature. Nevertheless, for $LaCoO_3$, the MIT is not sharp and smoothly spreads over a large temperature range of several hundreds of degrees. To our knowledge, no long range ordering has been found at low temperature. From a structural point of view, it should be emphasized that $TlSr_2CoO_5$ differs greatly from $LaCoO_3$ in the large elongation of the CoO_6 octahedra. This elongation can be associated with the layer-type structure of $TlSr_2CoO_5$, which contrasts with the more isotropic perovskite-type structure of $LaCoO_3$.

Fig. 15 shows the possible electronic configurations of Co^{3+}. The low spin (LS) state is generally stabilized in octahedral sites where the six Co–O distances are short and equal, as in $LiCoO_2$ or $CuCoO_2$. Clearly, the huge elongation of site I should favor a strong drop in the energy of the d_{z^2} level and a shrinking of the equatorial Co–O distances should raise the $d_{x^2-y^2}$ orbitals to a much higher energy. This prediction has been confirmed by tight binding extended Hückel calculations[17] (Fig. 16) which lead to the conclusion that, in site I, Co^{3+} ions exhibit an intermediate spin (IS) configuration ($S=1$). For site II, the variation in the Co–O distances is much smaller than for site I and the splitting of e_g orbitals due to octahedral distortion is also much smaller, as seen in Fig. 16. Hence a HS state is expected. The spin state of Co^{3+} in the HT-phase is more complex, especially since it must account for the metallic character, and has been discussed elsewhere on the basis of physical properties, including a Mössbauer investigation of a ^{57}Fe-doped sample.[18] The spin state can be described as a fluctuating mixture of IS and HS configurations. This mixed configuration disproportionates at the transition into localized IS and HS configurations. The corresponding I and II sites are well ordered thanks to the commensurate modulation of the oxygen positions in the o-phase. Drawing the ($\boldsymbol{a}_o$, $\boldsymbol{b}_o$) plane at the $z=0$ level for several cells allows the zigzag chains of II sites extending along the $\boldsymbol{a}_o$ direction separated by isolated I sites to be seen (Fig. 17). This picture resembles the stripes resulting from charge ordering (CO) in recently investigated mixed valence systems.[19] For this reason, we introduce here the concept of *spin state ordering* (SSO). In a similar way to

charge disproportionation and CO effects, SSD and SSO account well for the correlation between the metal–insulator transition and the structural change.

5 Conclusions

Although a first-order phase transition has been found for $TlSr_2CoO_5$ at room temperature, only a sharp shrinking of the unit cell upon heating was found in a preliminary investigation. The present work shows that a change of symmetry actually occurs at the transition. The main effect is the occurrence of a commensurate modulation of the position of the oxygen atoms which, in turn, leads to the formation of two sites for Co^{3+} ions at low temperature (against a single one at high temperature) strongly differing in the distribution of Co–O distances. The features of the structure modulation will be more accurately determined using neutron diffraction in a forthcoming study. This segregation of Co atoms does not correspond to a charge disproportionation, but to a spin state disproportionation. This structural change is clearly correlated with the change in electronic properties, explaining why the metallic character of the HT-phase is not present in the low temperature phase. In order to describe the situation in the LT-phase, the concept of spin state ordering (SSO) has been introduced and compared with charge ordering and the formation of stripes, discovered a few years ago in copper, nickel and manganese complex oxides.

References

1 M. Coutanceau, J. P. Doumerc, J. C. Grenier, M. Pouchard and D. Sedmidubsky, *Solid State Commun.*, 1995, **96**, 56.
2 M. Coutanceau, J. P. Doumerc, J. C. Grenier, P. Maestro, M. Pouchard and T. Seguelong, *C. R. Acad. Sci. (Paris)*, 1995, **320**, 675.
3 Service Central d'Analyses, CNRS, BP 22, F-69390 Vernaison, France.
4 http://www.lure.u-psud.fr/Experiences/PE_DCI_ENG.HTM
5 A. K. Ganguli and M. A. Subramanian, *J. Solid State Chem.*, 1991, **93**, 250.
6 J. Rodriguez-Carvajal, FullProf Program, ILL, Grenoble, 1995.
7 J. S. Kim, J. S. Swinnea and H. Steinfink, *J. Less-Common Met.*, 1989, **156**, 347.
8 M. Hervieu, C. Michel and B. Raveau, in *Thallium-Based High-Temperature Superconductors*, ed. A. M. Herman and J. V. Yakhmi, Marcel Dekker Inc., New York, 1993, p. 41.
9 R. Beyers, S. S. P. Parkin, V. Y. Lee, A. I. Nazzal, R. Savoy, G. Gorman, T. C. Huang and S. La Placa, *Appl. Phys. Lett.*, 1988, **53**, 432.
10 T. Seguelong, P. Maestro, J. C. Grenier, L. Fournès and M. Pouchard, *Physica B*, 1995, **215**, 427.
11 R. V. von Schenck and H. Müller-Buschbaum, *Z. Anorg. Allg. Chem.*, 1974, **403**, 197.
12 R. V. von Schenck and H. Müller-Buschbaum, *Z. Anorg. Allg. Chem.*, 1973, **396**, 111.
13 M. Coutanceau, J.-P. Doumerc, M. Chambon and J.-C. Grenier, *C. R. Acad. Sci. (Paris)*, 1995, **320**, 531.
14 M. Coutanceau, Thesis, Bordeaux I University, 1996, No. 1631.
15 J. B. Goodenough, *J. Phys. Chem. Solids*, 1958, **6**, 287.
16 M. A. Señaris-Rodríguez and J. B. Goodenough, *J. Solid State Chem.*, 1995, **116**, 224.
17 J.-P. Doumerc, J.-C. Grenier, P. Hagenmuller, M. Pouchard and A. Villesuzanne, *J. Solid State Chem.*, 1999, **147**, 211.
18 J.-P. Doumerc, M. Coutanceau, L. Fournès, J.-C. Grenier, M. Pouchard and A. Wattiaux, *C. R. Acad. Sci. (Paris)*, 2000, **2**, 637.
19 J. M. Tranquada, B. Sternlieb, J. D. Axe, Y. Nakamura and S. Uchida, *Nature*, 1995, **375**, 561.